3D Instability of Miscible Displacements in a Hele-Shaw Cell

E. Lajeunesse, J. Martin, N. Rakotomalala, and D. Salin

Laboratoire Fluides Automatique et Systèmes Thermiques, Bâtiment 502, Campus Universitaire, 91405 Orsay Cedex, France*

(Received 21 March 1997; revised manuscript received 12 September 1997)

We study the downward miscible displacement of a fluid by a lighter and less viscous one in the gap of a Hele-Shaw cell. For sufficiently large velocities, a well-defined interface separates the two fluids. As long as the velocity or the viscosity ratio are below a critical value, the interface has the shape of a tongue symmetric across the gap. For viscosity ratios larger than a critical value, estimated at 1.5, there exists a critical velocity, above which the interface becomes unstable, leading to a new 3D pattern involving regularly spaced fingers of wavelength about 5 times the cell thickness. We delineate the stability diagram. [S0031-9007(97)04791-1]

PACS numbers: 47.20.Gv, 47.20.Bp, 83.85.Pt

A key issue in interface dynamics is the understanding of pattern selection. Of particular interest is the pattern selection related to the 2D Saffman-Taylor finger (ST) [1], the selection rule of which has raised a great amount of interest [1–5]. ST dynamics govern a variety of seemingly different physical phenomena, such as viscous fingering [2], directional solidification [3], or thermal plume [4]. We recall that the well-studied ST finger results from the displacement of a viscous fluid by an immiscible, less viscous one in a Hele-Shaw cell (consisting of two parallel plates $L \times W$, separated by a small gap b). In this immiscible displacement problem, the interface in the gap consists of a nearly hemispherical meniscus, which completely spans the cell gap at the edges of the finger [6], provided that the capillary number ($\mathrm{Ca} = \eta q/\gamma$, with η the viscosity, γ the surface tension, and q the fluid velocity) is sufficiently small. The patterns resulting from the balance between capillary and viscous forces are by necessity quasi-2D (namely, in the $L \times W$ plane). The removal of surface tension, which makes the coexistence of the fluids across the gap possible, provides the opportunity to obtain 3D patterns, also extending across the gap. The existence of such patterns has an interest of its own, as well as in connection to the 2D selection rule discussed above. 3D patterns can be achieved using two miscible fluids, provided that the displacement velocity (i.e., the Peclet number, $\mathrm{Pe} = qb/D_m$, where D_m is the molecular diffusion coefficient) is sufficiently large for diffusion effects to be negligible [7,8], so that a sharp fluid interface can be defined. So far, only two specific experiments have addressed miscible displacements in a Hele-Shaw cell: gravity-driven flow in a rectangular geometry [9] and viscous fingering in a horizontal radial geometry (Paterson [10]). However promising Paterson's flower pattern might have been, his pioneering work was surprisingly not resumed even for the simple geometry of a rectangular cell.

This Letter presents experimental results of miscible displacements in a vertical planar Hele-Shaw cell in the high Pe regime and emphasizes the role that displacement features along the gap have on the overall pattern. Depending on the velocity and viscosity ratio M ($M = \eta_1/\eta_2 > 1$, where η_1 and η_2 denote the dynamical viscosities of initial and injected fluid, respectively), two new regimes are identified. For $M < M_c$ (where $M_c \approx 1.5$), or for velocities below a critical when $M > M_c$, the interface shape across the gap $L \times b$ is tonguelike, but is invariant in the W direction (namely, this is a stable 2D regime). However, for $M > M_c$ and a velocity exceeding a critical value, which depends on M, a 3D fingering pattern develops (unstable 3D regime) involving fingers regularly spaced along the W direction. Neither the existence of the specific threshold M_c, nor the fingering pattern can be obtained from high Ca limit of the 2D ST fingering [1,11]. We focus on the salient features of the experimental results and on a simplified analysis to estimate the critical velocity.

The vertical Hele-Shaw cell consists of two parallel plates of length $L = 80$ cm and width $W = 10$ cm, separated by a uniform spacer which ensures a gap of thickness $b = 1$ or 1.92 mm (Fig. 1). We denote the coordinate axes as x, y, z (with x oriented in the direction of gravity). We use silicone oils as miscible fluids, which allow us to cover three decades in the viscosity ratio, M, with a density contrast ranging from 1% to 10%. The molecular diffusivity D_m, measured for each pair of fluids using the deviation of a laser beam [12], ranges from 5 to $12.5 \times 10^{-7}\,\mathrm{cm}^2/\mathrm{s}$. These surprisingly low values have also been confirmed by conducting Taylor dispersion [13] measurements in the cell (in the low flow regime where transverse molecular diffusion and advection by the flow are equally important in mixing the fluids). To obtain an initially flat horizontal interface (in the $W \times b$ plane), the cell is partially filled from the bottom with the heavier and more viscous fluid. Then, the second fluid is introduced from the top. A stabilizing density difference yields a flat interface. As this procedure takes a few minutes to complete, diffusion causes the initial interface to extend somewhat (by about 0.1 mm) in the L direction. Subsequently, the displacing fluid is injected at a constant flow rate, which fixes the average velocity

 0031-9007/97/79(26)/5254(4)$10.00

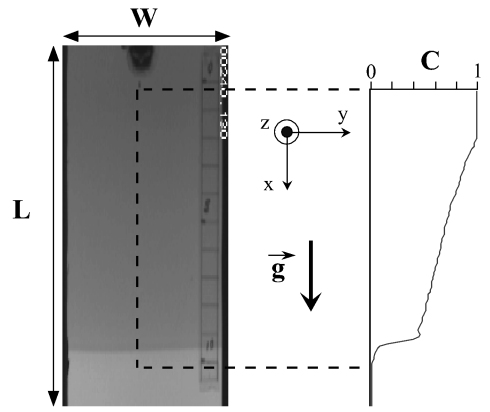

FIG. 1. Left: The 80 cm × 10 cm Hele-Shaw cell. Right: The average concentration across the gap b ($b = 1$ mm).

and the Pe number. A blue dye with diffusion coefficient close to that of the fluids is added to the injected fluid for visualization purposes. The average concentration across the gap, $C(x, y, t) = \int_0^b c(x, y, z, t)\, dz/b$ is measured using an optical video system. Figure 1 is a sketch of the cell and of a typical stable concentration profile in the experiment. The average concentration profile $C(x, y, t)$ is constructed from the $L \times W$ video picture (Fig. 1, left), using a calibration method which leads to an overall accuracy of the order of a few percent.

Experiments, with fluids of different viscosities, η, and densities, ρ, were performed at different flow rates, q, sufficiently high to satisfy $\mathrm{Pe} > 10^4$. In this regime, advection by the flow is predominant over diffusive mixing and the interface between the two fluids remains well defined [7,8]. Then, the main control parameters in the experiments are the viscosity ratio, M, and the normalized velocity $U = q/U_g$, where $U_g = (\rho_1 - \rho_2)gb^2/12\eta_1$ is the characteristic gravitational velocity. Thus, U expresses the ratio between viscous effects and buoyancy.

The experiment shown in Fig. 1 ($M = 5.8$, $U = 0.85$) is typical of the stable 2D regime; the concentration profile is invariant along the W direction, and the fluid interface has a symmetric tonguelike shape in the cross section $L \times b$. As we can only measure the average concentration across the gap, an experimental way to ascertain that the fluids do not mix by diffusion is to interrupt injection. This results in the shrinking of the concentration profile, and the return, under the action of gravity, to an almost flat interface in the $W \times b$ plane. We conclude that the fluids do not mix by diffusion and that the measured average concentration C is the relative amount of the injected fluid 2 in the gap. From the numerical simulations [7,8], we can further assume that the injected fluid is confined in the middle of the gap. Therefore, the flow pattern consists of a symmetric 2D tongue developing in the gap of the cell across the b direction.

When the viscosity ratio and the flow rate exceed certain thresholds M_c and $U_c(M)$, however, an unstable 3D regime, consisting of fingers regularly spaced along the W direction (Fig. 2), is observed. Assuming that the fluid interface is symmetric across the gap, the 3D shape of the fingers can be obtained from the $C(x, y)$ measurements. These develop along the primary flow direction, have a constant quasirectangular cross section, and are separated by a tiny layer of invaded fluid. It is interesting to note that their shape in the $L \times W$ plane is reminiscent of 2D directional solidification patterns [3]. Their width along the W direction, λ, and their thickness along the gap, τ, were measured for the two cell gaps b and for viscosity ratios M varying from 3 to 300. They were found to be nearly independent of M and to scale with b as follows:

$$\lambda = (5 \pm 1)b \quad \text{and} \quad \tau = (0.5 \pm 0.1)b\,. \qquad (1)$$

This value of λ is found to be comparable to the lower limit $\lambda = 4b$ obtained by Paterson [10] in his radial experiments. However, his results actually pertain to the rather disordered pattern obtained at $U \gg U_c$, which consists of less regular fingers, some of which predominate and screen the others.

The critical velocity U_c was measured for the two cell thicknesses using several fluids in order to get different types of variations of $\Delta\rho$ and η_1 with M. It was found that for $\mathrm{Pe} > 10^4$, the experimental values of $U_c(M)$ all collapsed into a single curve (Fig. 3), thus validating the velocity scaling used. This curve exhibits an interesting behavior at lower M values. For example, whereas $U_c(2.4) = 18$, it was not possible to reach the 3D regime for $M = 2.2$, even with the attempted velocity of 125 (arrow in Fig. 3). This suggests the existence of a viscosity ratio threshold, in the vicinity of 2, below which no 3D fingering occurs. This new result differs from the immiscible fluids case, where the viscous fingering threshold is $M = 1$ [1–3,5].

To interpret the behavior found, an obvious first approach would be to consider the classical linear stability for a Hele-Shaw cell [1], in the absence of surface tension and diffusion. Under these conditions and assuming that single-phase fluids fill the gap on opposite sides of the interface, this analysis leads to the critical flow rate

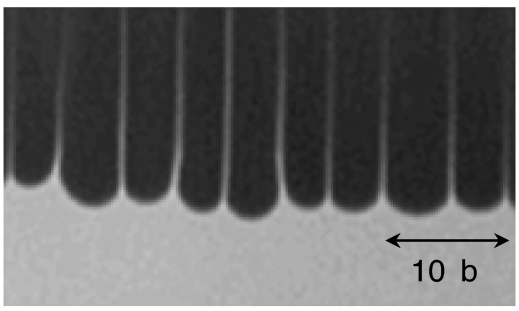

FIG. 2. 3D viscous fingering. The mean wavelength of the series of fingers is 5 times the gap thickness b.

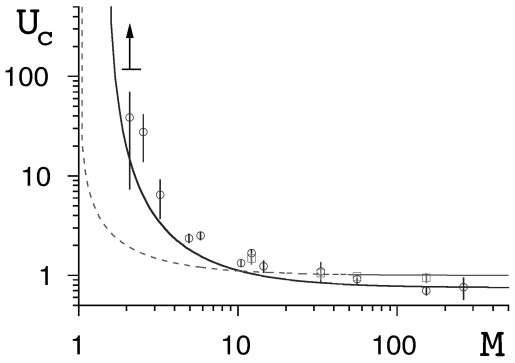

FIG. 3. Stability diagram: reduced velocity versus viscosity ratio M (log-log scale). Circles and squares correspond, respectively, to the cell thickness $b = 1$ and 1.92 mm. The dashed and full curves are theoretical. The arrow corresponds to the lower-bound velocity below which it was not possible to observe the 3D fingering.

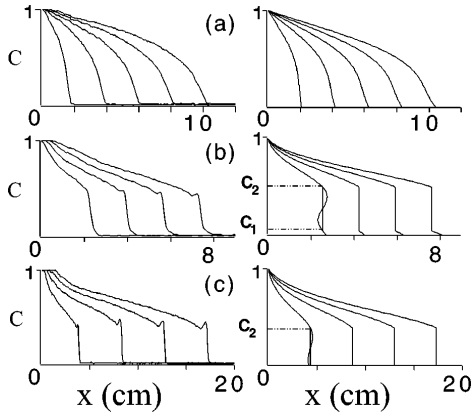

FIG. 4. Typical experimental (left) and calculated (right) concentration profiles, plotted at regular time intervals Δt. (a) $M = 1.1 < M_c$, $U = 3.2$, $\Delta t = 1$ s; (b) $M = 5.8 > M_c$, $U = 0.85 < U_c$, $\Delta t = 40$ s; (c) $M = 5.8$, $U = 2.55 > U_c$, $\Delta t = 30$ s.

$q_c = \frac{b^2}{12}\frac{(\rho_1-\rho_2)g}{(\eta_1-\eta_2)}$. The corresponding normalized critical velocity is then $U_c = M/(M-1)$ (Fig. 3, dashed line), which has a viscosity threshold $M_c = 1$. In the presence of a film of the displaced fluid left behind, as is the case in our experiment, a better approach is to use effective densities and viscosities (averaged across the gap), as considered by Saffman and Taylor [1] in their Appendix. Although leading to a higher value of U_c, however, these calculations still yield the same viscosity threshold ($M_c = 1$), whatever the value $(1 - C)$ of the film fraction. It is obvious that the conventional 2D approach cannot account for the experimentally observed thresholds for the case of miscible fluids, where the critical viscosity ratio found is certainly greater than 1. It appears that a more complex process actually occurs, in which the profile along the gap must be considered. To gain an insight, we will consider the features of the 2D base state, namely, a tongue advancing symmetrically in the gap.

This 2D interface can be experimentally obtained from the profile $C(x)$. Because of the symmetry along the gap, $C(x)$ also represents half the shape of this tongue. The plots on the left-hand side of Fig. 4 show three typical profiles $C(x)$ measured for $M < M_c$ (a), $M > M_c$ and $U < U_c$ (b), and $M > M_c$ and $U > U_c$ (c). Note that in the latter case, the flow pattern is not invariant along the W direction (where now a 3D instability develops), and here $C(x)$ is measured along the middle of a finger. In all cases, the concentration profile is found to be self-similar $[C(x,t) \equiv C(x/t)]$, which implies that each concentration travels at its own velocity $v(C) = \left(\frac{\partial x}{\partial t}\right)_C$.

However, different features characterize each of the three cases. In case (a), every point of the profile spreads in time (the profile is self-spreading) and $v(C)$ decreases monotonically with C. In case (b), there is in addition a region of intermediate concentrations ($0 < C_1 \leq C \leq C_2$), which propagate at the same velocity (sharp portion in the profile). Concentrations upstream and downstream of this front spread as in case (a). In particular, there exists a self-spreading tip ahead of the front. Case (c) is similar to case (b), except that the range of concentrations of constant velocity extends down to $C_1 = 0$: the time-spreading tip at the leading edge of the profile in case (b) has disappeared.

The existence of these different profile features suggests that an analysis of the 2D profile may be useful in providing estimates of the critical values M_c and U_c, without doing the complete 3D stability analysis. To do this, we follow the recent approach of Yang and Yortsos (YY) [8]. YY addressed analytically the 2D problem of the interface shape between two miscible fluids flowing between two parallel plates, in the absence of buoyancy and diffusion (Pe $\rightarrow \infty$). In parallel flow, the velocity profile is of the Haagen-Poiseuille type, from which the authors derived a first-order hyperbolic equation involving the flux function $f_M(C)$. The solution to this equation leads to self-similar concentration profiles [14] consisting either of self-spreading ones, with $v(C) = f'_M(C)$ [as in case (a)], or a combination of self-spreading and iso-velocity portions, denoted as shocks [as in case (b)]. Notably, YY found that a shock appears only if $M \geq 1.5$. Here, we extended these calculations by also introducing buoyancy. This leads to a normalized flux function which depends on both M and U. The right-hand-side plots of Fig. 4 show profiles calculated using this approach, and corresponding to the experiments in the left of Fig. 4. For $M \leq 1.5$ (a), the calculated self-spreading profile is in good quantitative agreement with the experiments. For $M > 1.5$ and U smaller than a critical value (b), the calculated profile exhibits a shock between C_1 and C_2, traveling with a normalized shock velocity V_s. The calculations reproduce well the experimentally observed tiny tip between $C = 0$ and C_1, which corresponds to a self-spreading behavior. Furthermore, the normalized tip front velocity, V_t (the zero concentration velocity), derived from the

calculations is $V_t = 1.5U$ [8] and fits well the experimental values. The theoretical analysis predicts that as U increases, the shock velocity V_s also increases, while at the same time the extent of the small tip decreases and ultimately vanishes at the critical flow rate corresponding to $V_s = V_t = 1.5U_c$. Thus, U_c determines the transition between cases (b) and (c), and therefore, we believe, the onset of the 3D instability. From the analysis (the details of which will be presented in a separate publication), we obtain the following analytical expression for U_c:

$$U_c = \frac{8M^3}{(2M - 3)^2(4M - 3)}. \qquad (2)$$

This expression shows a critical viscosity ratio $M_c = 1.5$, in better agreement with the experimental threshold M_c than the value $M_c = 1$ given by the ST analysis. The predictions of Eq. (2) for U_c are plotted as a full line in Fig. 3. They are in generally good agreement with our data, although somewhat lower. We believe that this slight deviation is due to the finite value of Pe in our experiments. In other sets of experiments involving lower values of Pe (for example, Pe $\simeq 5 \times 10^3$), we observed an increase of the critical velocity to values above those reported here. We believe then that the expression (2) for $U_c(M)$, which formally applies to Pe $\rightarrow \infty$, is a theoretical lower bound to the experimental data. We emphasize again that the above approach does not constitute a stability analysis, which still needs to be done. However, the definition of U_c from our 2D analysis provides information on the cause of the 3D instability. Indeed, consider the application of the above analysis to velocity values above U_c. This would result in an abrupt nose (shock) traveling at a velocity V_s larger than $1.5U$ (as also found in [8] in the absence of buoyancy). This velocity being larger than the maximum velocity existing in the displaced fluid ahead of the tongue (recall that the latter has a Poiseuille-type profile with maximum centerline velocity $1.5U$, in our notation) introduces a vorticity, which would lead to recirculation at the tip of the nose. We believe that this is the origin of the observed interface instability, which then results in the expansion of the flow pattern in the W direction.

In conclusion, we have studied the downward miscible displacement of one fluid by a lighter and less viscous one in a Hele-Shaw cell using as control parameters the viscosity ratio and the flow velocity. The latter is sufficiently large to prevent significant mixing by diffusion, and therefore the interface between the two fluids remains sharp and well defined. If either of the control parameters is smaller than a critical value, the flow pattern obtained is 2D and the shape of the interface is a tongue of the injected fluid spreading in the middle of the gap of the cell. Above a threshold in both the flow velocity $[U_c(M)]$ and the viscosity ratio ($M_c \simeq 1.5$), a 3D pattern develops as a series of periodic fingers (with $\lambda \simeq 5b$) of a regular cross section ($\simeq 5b \times 0.5b$). Simple arguments based on the parallel flow analysis of Yang and Yortsos [8] lead to an analytical description of the 2D regime. Using this approach and an experimental profile criterion (namely, $V_s = 1.5U_c$) allows us to determine the onset of instability, in agreement with the experiments.

The effect of the higher dimensionality of flow (3D vs 2D) on the critical thresholds for instability, as well as the properties of the patterns obtained, is quite interesting and should affect a broad class of processes which share the same mechanisms, such as solidification. How the increase in dimensionality affects the pattern selection rule (which in 2D has attracted significant attention) is also important and needs further study.

We are indebted to Professor M. Rabaud, Professor Y. C. Yortsos, and to G. Trinchero and P. Watzky for stimulating discussions.

*Université P&M Curie and Université Paris Sud associated with C.N.R.S. (URA 871).

[1] P. G. Saffman and G. I. Taylor, Proc. R. Soc. London A **245**, 312 (1958).
[2] D. Bensimon, L. P. Kadanoff, S. Liang, B. I. Shraiman, and C. Tang, Rev. Mod. Phys. **58**, 977 (1986); G. M. Homsy, Annu. Rev. Fluid Mech. **19**, 271 (1987).
[3] P. Pelcé, *Dynamics of Curved Fronts* (Academic Press, New York, 1988).
[4] G. Zocchi, P. Tabeling, and M. Ben Amar, Phys. Rev. Lett. **69**, 601 (1992).
[5] J. W. McLean and P. G. Saffman, J. Fluid Mech. **102**, 455 (1981); D. A. Kessler, J. Koplik, and H. Levine, Adv. Phys. **37**, 255 (1988); R. Combescot, T. Dombre, V. Hakim, Y. Pomeau, and A. Pumir, Phys. Rev. A **37**, 1270 (1988); D. Bonn, H. Kellay, M. Ben Amar, and J. Meunier, Phys. Rev. Lett. **75**, 2132 (1995).
[6] C. W. Park and G. M. Homsy, Phys. Fluids **28**, 1583 (1985).
[7] P. Petitjeans and T. Maxworthy, J. Fluid Mech. **326**, 37 (1996); C. Y. Chen and E. Meiburg, *ibid.* **326**, 57 (1996); N. Rakotomalala, D. Salin, and P. Watzky, *ibid.* **338**, 277 (1997).
[8] Z. Yang and Y. C. Yortsos, Phys. Fluids **9**, 286 (1997).
[9] R. A. Wooding, J. Fluid Mech. **39**, 477 (1969).
[10] L. Paterson, Phys. Fluids **28**, 26 (1985).
[11] A. Arneodo, Y. Couder, G. Grasseau, V. Hakim, and M. Rabaud, Phys. Rev. Lett. **63**, 984 (1989).
[12] A. Sommerfeld, *Optics, Lectures on Theoretical Physics IV* (Academic Press, New York, 1954).
[13] G. I. Taylor, Proc. R. Soc. London A **219**, 186 (1953).
[14] A. Jeffrey, *Quasilinear Hyperbolic Systems and Waves* (Pitman, London, 1976).